Macromolecules

ARTICLE

pubs.acs.org/Macromolecules

Influences of Hydrogen Bonding and Peripheral Chain Length on Mesophase Structures of Mesogen-Jacketed Liquid Crystalline Polymers with Amide Side-Chain Linkages

Yan-Hua Cheng,[†,‡] Wen-Ping Chen,[‡] Zhihao Shen,[*,†] Xing-He Fan,[*,†] Mei-Fang Zhu,[*,‡] and Qi-Feng Zhou[†]

[†]Beijing National Laboratory for Molecular Sciences, Key Laboratory of Polymer Chemistry and Physics of Ministry of Education, College of Chemistry and Molecular Engineering, Peking University, Beijing 100871, China

[‡]State Key Laboratory for Modification of Chemical Fibers and Polymer Materials, Donghua University, Shanghai 201620, China

ABSTRACT: A series of mesogen-jacketed liquid crystalline polymers, poly{2,5-bis-[(4-alkoxyphenyl)aminocarbonyl]styrene} (P-C*m*, where *m* is the number of carbon atoms in the alkoxy groups, and *m* = 1, 4, 8, 12), with an amide core and flexible tails of varying lengths on the two ends in the side chain were designed and successfully synthesized via conventional radical polymerization. The mesophase structures of these polymers were dependent on the number of carbon atoms in the peripheral chains. Wide-angle X-ray diffraction and polarized light microscopy results revealed that the polymers with $m \geq 4$ could form smectic A phases, while a columnar nematic phase could be formed for the polymer with methoxy end groups (P-C1). The hydrogen bonding among the side-chain amide groups might play an important role in forming and stabilizing these liquid crystalline phases, which was suggested by the results from variable-temperature FTIR and 2D IR analyses.

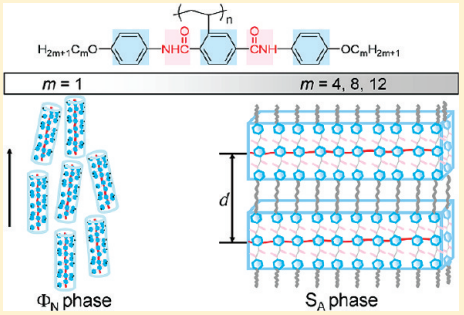

INTRODUCTION

Liquid crystalline polymers (LCPs) represent fascinating materials of soft matter, combining anisotropic properties on molecular and supramolecular levels and good mechanical properties on the whole. Such liquid crystalline (LC) ordering depends on external stimuli and is of great importance for numerous applications not only in materials science but also in biosystems.[1] Side-chain LC polymers (SCLCPs), depending on the position of the mesogens linking to the backbone, either longitudinally or laterally attached into the polymeric system, are called end-on or side-on SCLCPs.[2] In order to achieve liquid crystallinity, flexible spacers are usually introduced in SCLCPs to decouple the dynamics of the main chain and the mesogenic side groups.[3] In contrast to the conventional route to design SCLCPs, Zhou et al.[4] reported a special type of side-on SCLCPs called mesogen-jacketed liquid crystalline polymers (MJLCPs), which had a short spacer or with a single covalent bond connecting the mesogen to the polymer backbone. In our previous work, we have systematically investigated the syntheses and LC properties of MJLCPs,[5] revealing that the MJLCP chain acts like a supramolecular cylinder because of the so-called "jacketing" effect (the main chain takes an extended chain conformation due to the steric effect of the densely distributed bulky side groups), and many MJLCPs form columnar phases.[5−8] Recently, smectic phases have also been reported when the length or the rigidity of the mesogen was increased[9,10] or when semifluorinated tails were introduced into the mesogens.[11] The previous researches on MJLCP systems mostly focused on structures based on 2-vinylterephthalic acid with ester linkages.

To design LC materials with high complexity, versatility, and functionality, supramolecular chemistry is a viable and facile technique in building up complex systems based on noncovalent bonds, such as hydrogen bonding, ionic interaction, $\pi-\pi$ interaction, coordination interaction, van der Waals force, and so on.[12−14] The characteristics and advantages of such LC materials are that they can change their structures by the dynamic and reversible noncovalent interactions when responding to the different environment. Among these interactions, hydrogen bonding has been extensively explored to tailor self-assembled nanostructures for the applications in the fields of biology and materials science.[15−18]

Introducing amide groups, which can form hydrogen bonding, into MJLCPs might bring about a new way to control phase structures. Previously, we have synthesized 2-vinyl-1,4-phenylenediamine-based poly-2,5-bis(4-alkoxybenzamido)styrene, which exhibited a lyotropic nematic phase when methoxy groups were appended to the two ends of the mesogens.[19] However, because of the time-consuming procedure in synthesizing the polymers, their properties have not been fully investigated. Herein, we report a novel series of MJLCPs, which could be synthesized more conveniently, with amide linkages based on 2-vinylterephthalic acid.[20] Hydrogen bonding could be formed among the side-chain amide groups. The length of the peripheral alkoxy tails was varied in these poly{2,5-bis[(4-alkoxyphenyl)-aminocarbonyl]styrene} (P-C*m*, where *m* is the number of carbon

Received: October 27, 2010
Revised: January 20, 2011
Published: February 14, 2011

Scheme 1. Synthetic Route of Monomers and Polymers

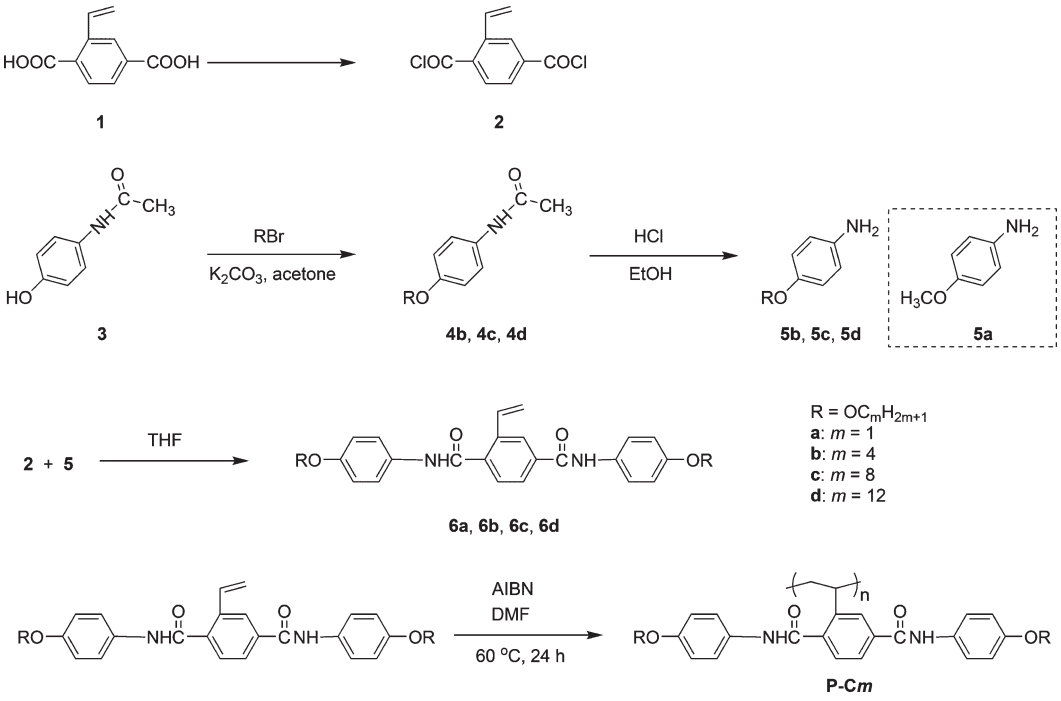

atoms in the alkoxy groups, and m = 1, 4, 8, 12) polymers. We examined the liquid crystallinity of these polymers using various techniques, such as X-ray diffraction and optical microscopy, and found that the LC phase structures were affected by both hydrogen bonding and the peripheral chain length.

EXPERIMENTAL SECTION

Materials. The compound vinylterephthalic acid was synthesized using the method previously reported.[20] 2,2′-Azobis(isobutyronitrile) (AIBN, Beijing Chemical Co., 95%) was purified by recrystallization from ethanol before use. *N,N*′-Dimethylformamide (DMF, Beijing Chemical Co., A.R.) used as the polymerization solvent was distilled over CaH_2 prior to use. Tetrahydrofuran (THF) and triethylamine (Et_3N) were refluxed over CaH_2 under argon and distilled out before use. Dichloromethane (Beijing Chemical Co., A.R.) was dried over anhydrous magnesium sulfate. All other reagents and solvents were used as received from commercial sources.

Measurements. ^{1}H NMR spectra, mass spectra (MS), gel permeation chromatographic (GPC) measurements, thermogravimetric analyses (TGA), differential scanning calorimetry (DSC), polarized light microscopy (PLM), and one-dimensional (1D) and two-dimensional (2D) wide-angle X-ray diffraction (WAXD) experiments were carried out according to the procedures described previously.[21]

Hydrogen bonding was studied using variable-temperature FTIR. The spectra were recorded on a Nicolet 8700 FTIR spectrometer with a resolution of 4 cm^{-1} using a variable-temperature cell, and 32 scans were coadded for each spectrum in the wavenumber range 400−4000 cm^{-1}. A sample of ~1.5 mg was sandwiched between two KBr windows.

Furthermore, 2D IR correlation analysis, which is a spectral analysis method originally proposed by Noda,[22] was carried out to probe the mechanism of the (LC) phase development. FTIR spectra collected in the temperature range 80−280 °C with a 10 °C interval were utilized to perform the 2D IR correlation analysis with the Omnic 7.2 SpectraCorr software.

Synthesis of Monomers. The synthetic route of the monomers, 2,5-bis[(4-alkoxyphenyl)aminocarbonyl]styrene (M-C*m*, where *m* is the number of carbon atoms in the alkoxy groups, and m = 1, 4, 8, 12), is shown in Scheme 1. The experimental details of monomer synthesis and characterization are described below using M-C12 as an example.

Synthesis of N-(4-Dodecyloxyphenyl)acetoamide, ***4d****.* A mixture of 4-acetoamidophenol (1.81 g, 12.0 mmol), 1-bromododecane (3.74 g, 15.0 mmol), and potassium carbonate (4.98 g, 36.0 mmol) in acetone (50 mL) was heated under reflux for 24 h. The excessive potassium carbonate was filtered off and washed with acetone for several times. After evaporation of the solvent, the residue was recrystallized from ethanol to give **4d** as a white crystal. ^{1}H NMR (300 MHz, $CDCl_3$, δ, ppm): 0.88 (t, 3H, $-CH_3$), 1.10−1.82 (m, 20H, $-CH_2-$), 2.15 (s, 3H, $CO-CH_3$), 3.92 (t, 2H, $-OCHH_2-$), 6,84 (d, 2H, Ar−H), 7.13 (br s, NH), 7.36 (d, 2H, Ar−H). Anal. Calcd for $C_{20}H_{33}NO_2$: C, 75.19; H, 10.41; N, 4.38. Found: C, 75.29; H, 10.32; N, 4.35.

Synthesis of 4-Dodecyloxyphenylamine, ***5d****.* An ethanol (35 mL) solution of **4d** (2.59 g, 8.12 mmol) and a dilute HCl aqueous solution were stirred at 75 °C. After 2 days, the solvent was evaporated in vacuo to obtain a white crystal, 4-dodecyloxyphenylamide hydrochloride. ^{1}H NMR (300 MHz, $CDCl_3$, δ, ppm,): 0.88 (t, 3H, $-CH_3$), 1.17−1.85 (m, 20H, $-CH_2-$), 3.93 (t, 2H, $-OCHH_2-$), 6.90 (d, 2H, Ar−H), 7.44 (d, 2H, Ar−H), 10.38 (br s, $NH_2\cdot HCl$). Anal. Calcd for $C_{18}H_{32}NOCl$: C, 68.87; H, 10.28; N, 4.46. Found: C, 68.90; H, 10.16; N, 4.48. Then an aqueous solution of $NaHCO_3$ (saturated, 50 mL) was added to 4-dodecyloxyphenylamide hydrochloride until the pH ≥ 7. The mixture was extracted with dichloromethane, and the extract was dried with anhydrous Na_2SO_4 and concentrated to give **5d**. After the purity of **5d** was tested by thin layer chromatography and ^{1}H NMR, it was directly used in the next step.

Synthesis of 2,5-Bis[(4-dodecyloxyphenyl)aminocarbonyl]styrene, ***6d****.* Vinylterephthalic acid (0.75 g, 3.90 mmol), 10 mL of oxalyl chloride, and a few drops of DMF were dissolved in dichloromethane (25 mL) in a 50 mL round-bottom flask. The mixture was stirred for 5 h. After evaporation of the solvent under reduced pressure, the residue was dissolved in anhydrous THF. The resultant light yellow solution of

dx.doi.org/10.1021/ma102444t |*Macromolecules* 2011, 44, 1429–1437

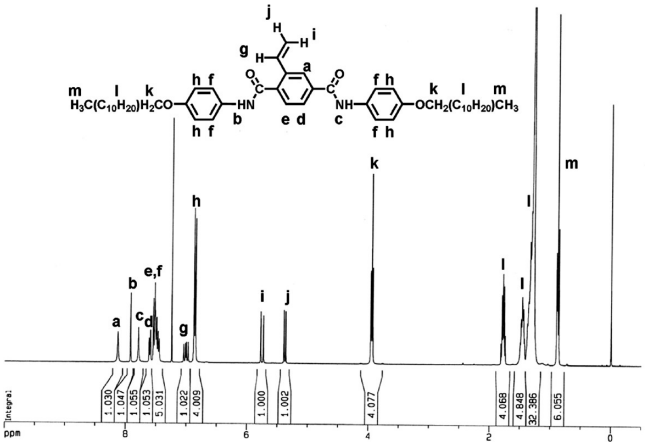

Figure 1. ^{1}H NMR spectrum of M-C12 in $CDCl_3$.

vinylterephthal chloride was slowly dropped into an intensely stirred solution of 50 mL of THF and 10 mL of triethylamine containing **5d** for 1 h in an ice/water bath. The solution was further stirred for 24 h at ambient temperature. After evaporation of the solvent, the residue was washed with water and recrystallized from THF/petroleum ether (1/1, v/v) with active carbon as the decolorant to obtain a white solid. Figure 1 shows the ^{1}H NMR of **6d** (M-C12) in deuterated chloroform. ^{1}H NMR (400 MHz, $CDCl_3$, δ, ppm,): 0.88 (t, 6H, $-CH_3$), 1.28−1.79 (m, 40H, $-CH_2-$), 3.95 (t, 4H, $-OCHH_2-$), 5.38 (d, 1H, $=CH_2$), 5.75 (d, 1H, $=CH_2$), 6.87 (d, 4H, Ar−H), 7.00 (q, 1H, −CH=), 7.45−7.60 (m, 5H, Ar−H), 7.61 (d, 1H, Ar−H), 7.79 (s, 1H, −NH−), 7.92 (s, 1H, −NH−), 8.13 (s, 1H, Ar−H). MS (EI): m/z 710. Anal. Calcd for $C_{46}H_{66}N_2O_4$: C, 77.70; H, 9.36; N, 3.94. Found: C, 76.96; H, 9.36; N, 3.86.

Compounds **6b** and **6c** were similarly prepared as mentioned for **6d**, while **6a** was prepared from commercially available **5a**.

2,5-Bis[(4-methyloxyphenyl)aminocarbonyl]styrene, ***6a***. ^{1}H NMR (400 MHz, DMSO-d_6, δ, ppm,): 3.75 (d, 6H, $-OCH_3$), 5.43 (d, 1H, $=CH_2$), 5.97 (d, 1H, $=CH_2$), 6.92 (d, 4H, Ar−H), 7.01 (q, 1H, −CH=), 7.59−7.70 (m, 5H, Ar−H), 7.94 (d, 1H, Ar−H), 8.25 (s, 1H, Ar−H), 10.15 (s, 1H, −NH−), 10.21 (s, 1H, −NH−). MS (EI): m/z 402. Anal. Calcd for $C_{24}H_{22}N_2O_4$: C, 71.63; H, 5.51; N, 6.96. Found: C, 71.08; H, 5.45; N, 6.75.

2,5-Bis[(4-butoxyphenyl)aminocarbonyl]styrene, ***6b***. ^{1}H NMR (400 MHz, DMSO-d_6, δ, ppm,): 0.94 (t, 6H, $-CH_3$), 1.41−1.47 (m, 4H, $-CH_2-$), 1.68−1.72 (m, 4H, $-CH_2-$), 3.95 (t, 4H, $-OCHH_2-$), 5.44 (d, 1H, $=CH_2$), 6.01 (d, 1H, $=CH_2$), 6.91−6.96 (m, 5H, Ar−H, −CH=), 7.61−7.70 (m, 5H, Ar−H), 7.94 (d, 1H, Ar−H), 8.28 (s, 1H, Ar−H), 10.27 (s, 1H, −NH−), 10.36 (s, 1H, −NH−). MS (EI): m/z 486. Anal. Calcd for $C_{30}H_{34}N_2O_4$: C, 74.05; H, 7.04; N, 5.76. Found: C, 73.45; H, 6.97; N, 5.69.

2,5-Bis[(4-octyloxyphenyl)aminocarbonyl]styrene, ***6c***. ^{1}H NMR (400 MHz, DMSO-d_6, δ, ppm,): 0.87 (t, 6H, $-CH_3$), 1.28−1.72 (m, 24H, $-CH_2-$), 3.95 (t, 4H, $-OCH_2-$), 5.43 (d, 1H, $=CH_2$), 5.97 (d, 1H, $=CH_2$), 6.89−6.93 (d, 4H, Ar−H), 7.01 (q, 1H, −CH=), 7.58−7.68 (m, 5H, Ar−H), 7.94 (d, 1H, Ar−H), 8.25 (s, 1H, Ar−H). MS (EI): m/z 598. Anal. Calcd for $C_{38}H_{50}N_2O_4$: C, 76.22; H, 8.42; N, 4.68. Found: C, 76.29; H, 8.37; N, 4.62.

Polymerization. As shown in Scheme 1, all polymers were obtained by conventional radical polymerization in solution. A typical polymerization procedure was carried out as the following, again, using P-C12 as an example. About 0.10 g (0.14 mmol) of M-C12, 10 μL of DMF solution of 0.08 M AIBN, and 1.9 mL of DMF/THF (1/1, v/v) were transferred into a polymerization tube. After three freeze−pump−thaw cycles, the tube was sealed off under vacuum. Polymerization was carried out at 60 °C for 24 h. The tube was then opened, and the reaction mixture was diluted with 10 mL of THF. The resultant polymer was precipitated and washed with methanol. To completely eliminate the unreacted monomer, the precipitate was redissolved in THF and then reprecipitated in methanol for three times. Finally, the polymer was dried to a constant weight.

Table 1. Molecular Weights, Polydispersity Indexes, and Thermal Properties of P-C*m*

sample	M_n ($\times 10^4$ g/mol)[a]	PDI[a]	T_d (°C)[b]	T_g (°C)[c]
P-C1	3.90	2.07	384	245
P-C4	3.14	2.18	390	222
P-C8	20.6	1.02	383	206
P-C12	6.90	1.57	413	199

[a] The apparent number-average molecular weight (M_n) and polydispersity index (PDI) were measured by GPC using PS standards. [b] The temperatures of 5% weight loss under nitrogen were measured by TGA heating experiments at a rate of 20 °C/min. [c] The glass transition temperatures were measured by DSC at a heating rate of 40 °C/min under a nitrogen atmosphere during the second heating process.

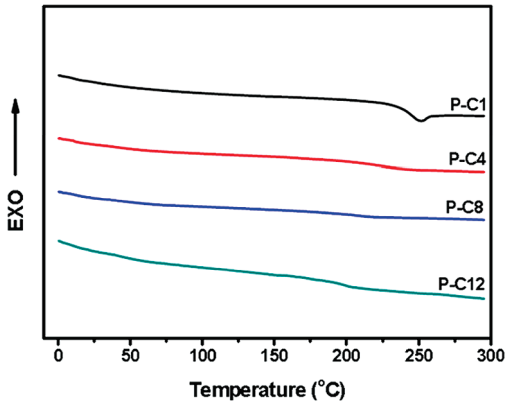

Figure 2. DSC thermograms of P-C*m*'s at a heating rate of 40 °C/min under a nitrogen atmosphere following cooling at 5 °C/min.

RESULTS AND DISCUSSION

Synthesis and Characterization of Monomers and Polymers. As shown in Scheme 1, the monomers were synthesized in four steps. The structures of the monomers were confirmed by conventional analyses, including ^{1}H NMR, elemental analysis, and mass spectrometry.

All the monomers were easily polymerized via the conventional radical polymerization method. The molecular characteristics of the polymers are summarized in Table 1. The apparent number-average molecular weights (M_n's) of the polymers determined by GPC were higher than 3 × 10^4 g/mol, demonstrating good polymerizability of the monomers. TGA measurements showed that all polymers were quite stable under a nitrogen atmosphere. The temperatures of 5% weight loss (T_d's) were all higher than 380 °C as shown in Table 1. The excellent thermal stability was probably due to the hydrogen bonds among the amide moieties.

Phase Transitions and Phase Structures. All polymers were amorphous when obtained from solution radical polymerization. The DSC experiments of P-C*m*'s were performed under a nitrogen atmosphere at a heating rate of 40 °C/min following a cooling process at a rate of 5 °C/min. Figure 2 shows DSC thermograms of P-C*m*'s. Only glass transitions could be observed, and the glass transition temperature (T_g) was dependent

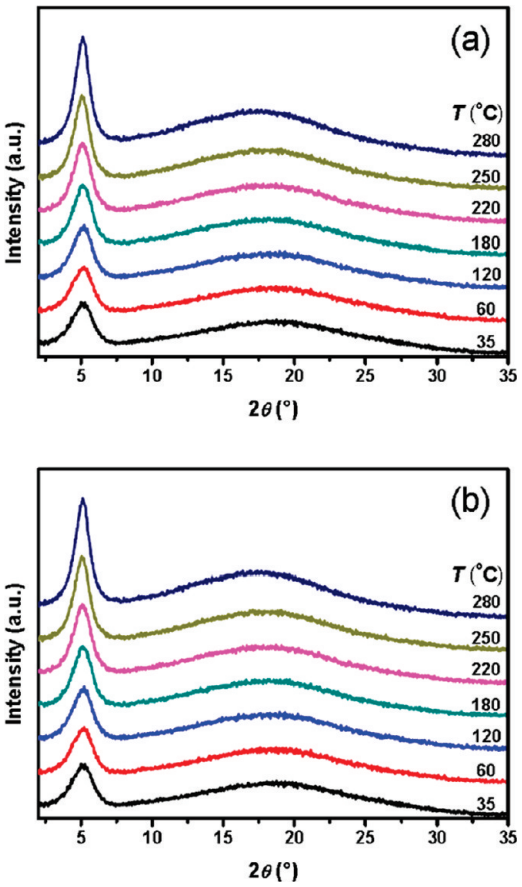

Figure 3. Sets of 1D WAXD patterns of P-C1 obtained during the first heating (a) and the first cooling (b) processes.

on the number of methylene groups, *m*, in the flexible alkyl tails for the P-C*m* series. T_g decreased with increasing alkyl chain length due to the increased plasticization by the alkyl end chains, as expected.

To study the phase transitions and the phase structures of P-C*m*'s at different temperatures, 1D WAXD experiments were performed. About 30 mg of the polymer was dissolved in acetone (for P-C1) or THF (for P-C4, P-C8, and P-C12) and cast onto a copper substrate, and then the solvent was allowed to evaporate at ambient temperature. The temperature was not higher than 280 °C during the experiments for all samples to avoid thermal degradation. Parts a and b of Figure 3 show two sets of 1D WAXD patterns of P-C1 during the first heating and the subsequent cooling processes, respectively. In Figure 3a, there were only two scattering halos in the low-angle and high-angle regions at 35 °C, indicating that P-C1 was in the amorphous state. The intensity of the low-angle halo increased upon the first heating to 280 °C and decreased upon the subsequent cooling (Figure 3b). It was difficult to judge whether there were phase transitions during heating and cooling from 1D WAXD experiments. On the other hand, *schlieren* texture started to develop at 278 °C (Figure 4a) when P-C1 was heated, and the texture remained during further cooling, indicating possible existence of an LC phase. Schlieren texture is frequently found in nematic and smectic C (S_C) phases, but not in smectic A (S_A) phases. In our pervious study, MJLCPs having smectic phases exhibit S_C phases only when relatively long alkyl chains are appended to the ends of the mesogens, while those with short alkyl ends exhibit S_A phases.[23]

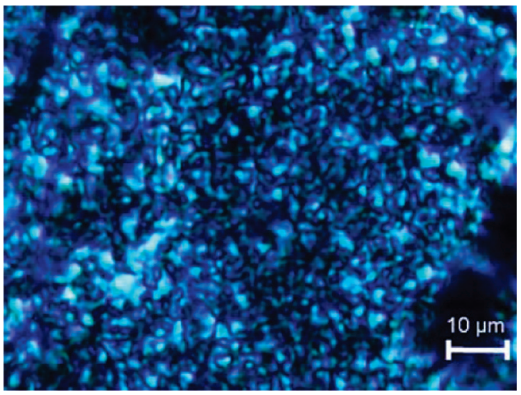

Figure 4. PLM micrograph of P-C1 at ambient temperature. The bulk sample was cooled from 280 °C.

Therefore, we assigned the phase structure of P-C1 to columnar nematic phase (Φ_N), which was a formed by the supramolecular rods of P-C1, although there might be other possibilities. The *d*-spacing of the low-angle halo was 1.68 nm at 35 °C during cooling. Thus, the columnar diameter was 1.94 nm, which was close to the simulated length (2.00 nm) of the side group.

When the number of methylene groups in the end chains was increased to 4, the segregation of the amide cores and the lipid end chains took place. This was reflected in the WAXD patterns of P-C4 as shown in Figure 5, which were different from those of P-C1. During first cooling from the high temperature of 270 to 250 °C, a sharp peak appeared at 2θ = 3.24°, indicating the existence of an ordered structure. However, the intensity of the low-angle diffraction did not increase with the further decrease in temperature. With annealing and heating back to 270 °C, the intensity increased significantly, as shown in Figure 5a. When the temperature was decreased to 250 °C again, two high-order diffraction peaks were observed (Figure 5b). The three diffraction peaks had 2θ values of 3.24°, 6.50°, and 9.76°, and the ratio of the scattering vectors of these three peaks was approximately 1:2:3, indicating a smectic structure of the sample P-C4, and the *d*-spacing of the low-angle diffraction peak represented d_{100} of the smectic phase. In addition, all these diffraction peaks almost retained their intensity during the cooling process similar to the cases of some other MJLCPs reported previously.[9,10] No noticeable change could be observed during the second heating and cooling processes in 1D WAXD experiments, implying that there was no isotropization for P-C4 in the temperature region we studied.

When *m* was further increased to 8 and 12, the polymers also formed smectic phases upon cooling from high temperatures, similar to P-C4. As mentioned before, the longer alkyl chains decreased the glass transition of the polymer due to the enhanced internal plasticization. The softening of the backbone could also be confirmed by the reduction of temperature in isotropization from the 1D WAXD experiments (Figure 6). One difference between P-C12 and P-C4 was that P-C12 went into the isotropic liquid at high temperatures, as reflected by the second heating and cooling processes in the 1D WAXD study in Figure 6a, although the transition could not be detected in DSC. After the glass transition, the low-angle scattering halo appeared, accompanied by the decrease in intensity of the sharp first-order diffraction peak, implying that the smectic phase started to disorder. At 280 °C, the sharp first-order diffraction peak completely disappeared, with only a scattering halo remaining, indicating that

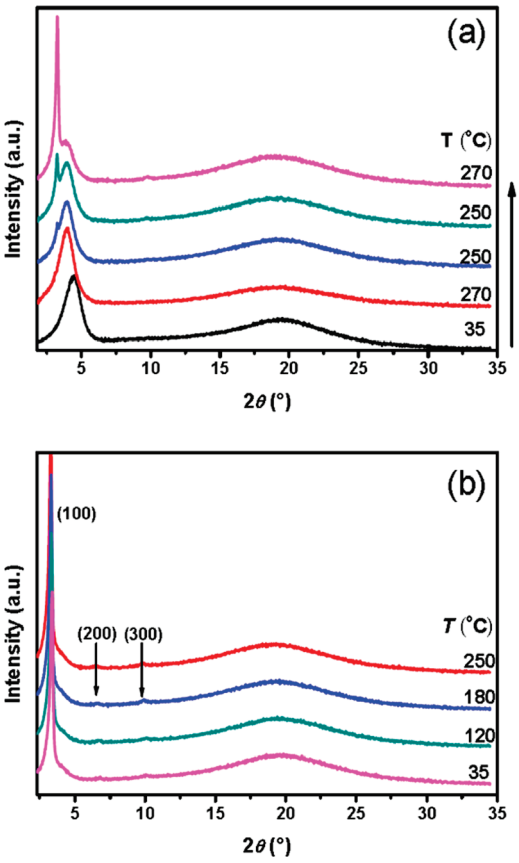

Figure 5. 1D WAXD patterns of P-C4 during the formation of the smectic phase (a), with the arrow pointing out the direction of temperature change, and the patterns recorded during the last cooling process (b).

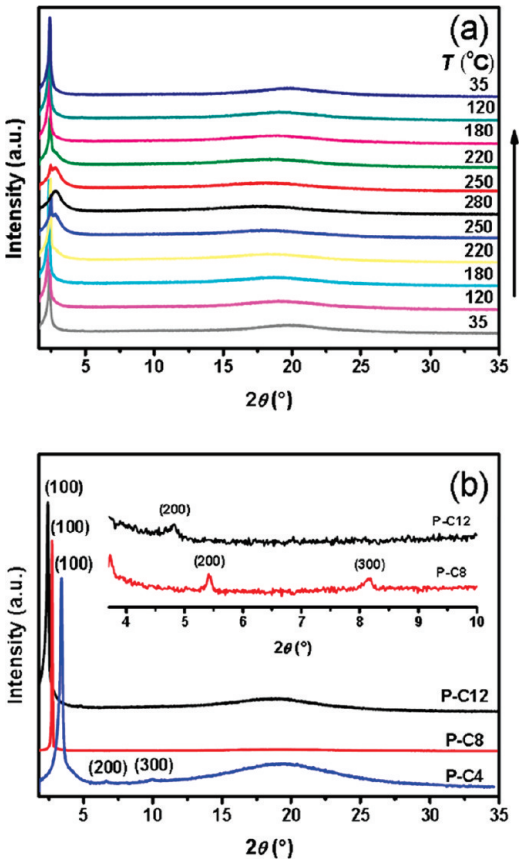

Figure 6. 1D WAXD patterns of P-C12 obtained during the second heating and subsequently cooling processes (a), with the arrow pointing out the direction of the temperature change, and the patterns for P-C4, PC-8, and P-C12 at 180 °C during cooling (b), with the inset showing the (200) and (300) diffractions.

the polymer entered into the isotropic state. The smectic LC phase formed again upon cooling. The phase behavior of P-C8 was similar to that of P-C12, although only partial disordering of the smectic phase of P-C8 could be observed at 280 °C, which was the highest temperature in our experiments in order to avoid thermal decomposition. We reasoned that the isotropization temperatures were higher than 280 °C for P-C8 and P-C4. The diffraction patterns of the smectic phases at 180 °C during the cooling process for all the samples are shown in Figure 6b. The layer spacing values of the polymers are listed in Table 2, which also increased with increasing length of the side chain, similar to the cases of other MJLCPs forming smectic phases.[9,10]

To identify the smectic structures of the polymers, 2D WAXD experiments were carried out. Taking P-C12 as an example, the oriented sample for the experiments was prepared by mechanically shearing the solution-cast film at 250 °C. The sample was put on the sample stage, and the point-focused X-ray beam was aligned perpendicular to the shear direction. Figure 7 shows the pattern of the sheared P-C12. A pair of strong low-angle diffraction arcs appeared on the equator, which was perpendicular to the shear direction, indicating that the normal of the smectic layers was perpendicular to the shear direction. Meanwhile, the high-angle scattering halo was more or less concentrated on the meridian with rather broad azimuthal distributions. The pattern in Figure 7 proved that the smectic phase of P-C12 was S_A instead of S_C. Similar patterns were obtained from samples of P-C4 and P-C8, suggesting that these two polymers also formed S_A phases.

As in other MJLCPs, the microphase separation between the flexible alkyl ends and the rigid core in the side chains might play an important role in the formation of LC phases. On the other hand, P-C4 formed an S_A phase, different from the hexatic columnar nematic phase of poly{2,5-bis[(4-butoxyphenyl)oxycarbonyl]-styrene}[24] which had the similar chemical structure to that of P-C4, but with ester linkages instead of amide linkages in the side groups. Therefore, the amide linkage could have an important effect in forming the smectic phase. Hydrogen bonding might exist among the amide linkages, resulting in more rigid side chains and more sheetlike conformation for the polymers, both of which favored the formation of smectic phases. It should be noted that all three samples (P-C4, P-C8, and P-C12) formed their S_A phases at an almost identical temperature, irrelevant to their alkyl end chain lengths. This phenomenon could be related to the effect of hydrogen bonding, which will be discussed in the following section. Contrary to increasing the rigidity of the side chain by increasing the length of the rigid core in the mesogen to form smectic phases, in the P-C*m* polymers, the side-chain hydrogen bonding was an important factor. However, for P-C1 with methoxy groups on two ends, a columnar nematic phase was formed. Therefore, both the hydrogen bonding and the terminal alkyl chains with enough lengths might be responsible for the formation of the observed S_A phases.

Molecular Origin of the Phase Transitions. To understand the role of the side-chain hydrogen bonding in phase transitions,

Table 2. Summary of X-ray Diffraction Results of P-C*m*'s

sample	molecular length of side chain (nm)[a]	layer spacing (nm)[b]	phase[c]	T_{LC} (°C)
P-C1	2.00		Φ_N	278[d]
P-C4	2.65	2.72	S_A	250[e]
P-C8	3.51	3.23	S_A	250[e]
P-C12	4.37	3.65	S_A	265−250[e]

[a] Molecular length calculated with the assumption of *all-trans* chain conformation. [b] Values of d_{100}. [c] Φ_N: columnar nematic phase; S_A: smectic A phase. [d] The temperature at which *schlieren* texture appeared under PLM during the heating process. [e] The temperature at which the sharp diffraction peak appeared in 1D WAXD experiments during the cooling process.

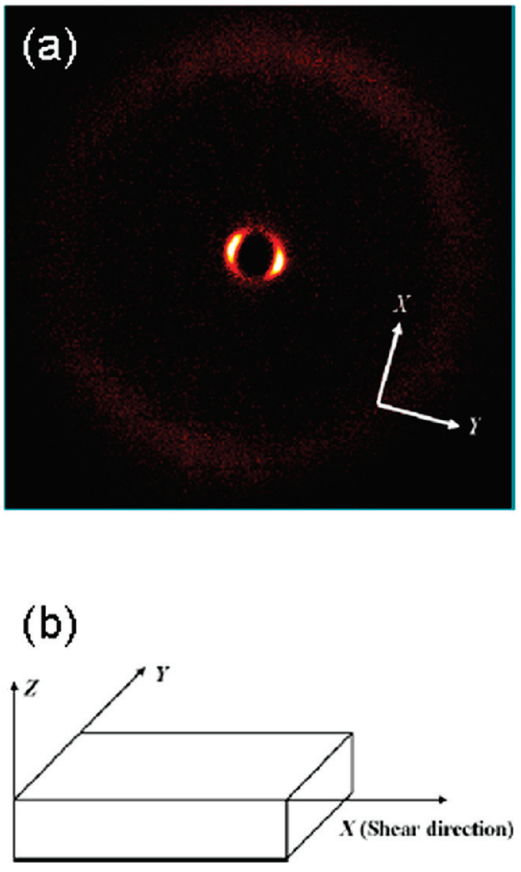

Figure 7. 2D WAXD pattern of P-C12 with the X-ray beam perpendicular to the shear direction (a) and the shearing geometry (b).

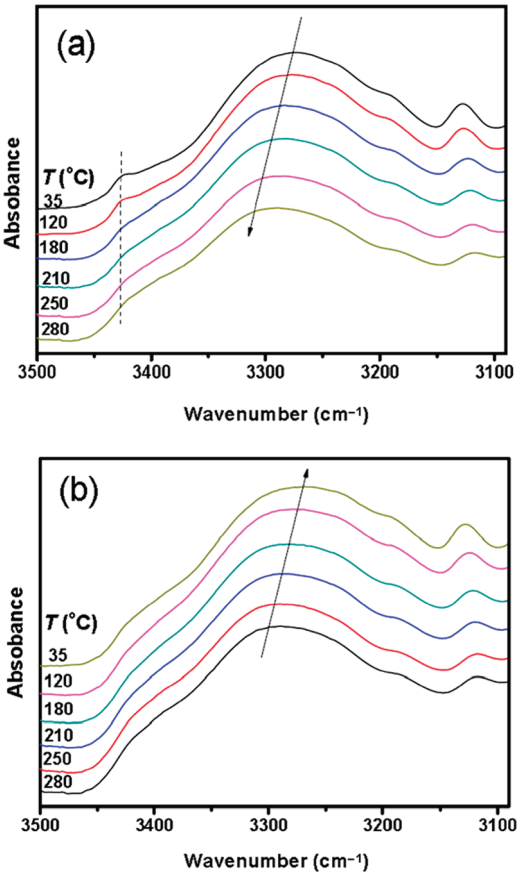

Figure 8. FTIR spectra of P-C12: N−H stretching region 3500−3090 cm^{-1} in the temperature range 35−280 °C during heating (a) and cooling (b).

we carried out variable-temperature FTIR experiments. The information about the hydrogen-bonding state was obtained from the N−H stretching (ν_{N-H}) vibration and amide I bands. Taking P-C12 as an example, it exhibited two infrared bands at 3426 cm^{-1} (weak shoulder) and 3275 cm^{-1} (very broad) of ν_{N-H} (Figure 8a), which were assigned to "free" (higher than 3400 cm^{-1}) and hydrogen-bonded N−H stretching modes, respectively. The peak positions of the absorption bands of ν_{N-H} and amide I (1652 cm^{-1}) clearly indicated that at ambient temperature most N−H groups were associated with the C═O groups, reflecting the presence of relatively strong hydrogen bonding.[25,26] The N−H stretching vibration was dependent on the temperature. The ν_{N-H} band became weaker and shifted toward higher frequencies upon heating to 280 °C, showing a very broad absorption band with a peak at 3292 cm^{-1}, which indicated that the hydrogen bonding became very weak in the isotropic state at 280 °C.[27] This is demonstrated in Figure 8a, which show representative FTIR spectra ("free" and hydrogen-bonded N−H stretching vibrations) for P-C12 at selected temperatures. The increased frequency of the N−H stretching band could be attributed to the decrease in the average strength of the hydrogen-bonded N−H groups. The intensity and frequency of the N−H stretching (ν_{N-H}) vibration absorption were recovered when the temperature was decreased (Figure 8b).

A similar phenomenon was also observed for other P-C*m* polymers. This temperature-dependent behavior could be rationalized by the following. Before the polymers were heated, there was relatively strong hydrogen bonding in these samples, which stabilized the nascent amorphous structures from the preparation process. However, the side-chain hydrogen bonding became weaker upon heating, which was necessary for the mesogenic molecules to obtain mobility in the amorphous state. Upon cooling, the hydrogen bonding was recovered, which enhanced

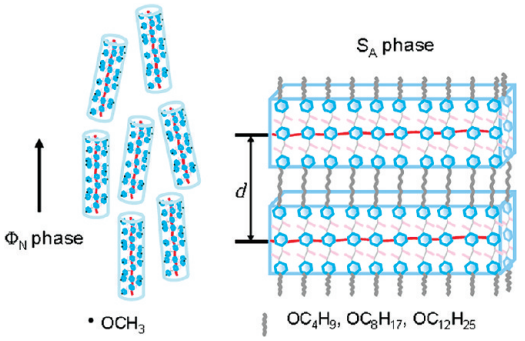

Figure 9. Schematic drawing of the LC phase structures of the polymers. P-C1 formed a columnar nematic phase, while P-C4, P-C8, and P-C12 formed S_A phases.

the attractive interaction between the neighboring mesogens to form an ordered phase. This dynamic and reversible nature of the hydrogen bonding was essential for the formation and stabilization of the LC phases.[28]

We also examined the band centered around 1600 cm^{-1} representing the C−C stretching mode of the benzene ring in P-C12, which slightly shifted toward lower frequencies from 1603 to 1596 cm^{-1} upon heating. The shifts might be related to the strengthening of the intermolecular $\pi-\pi$ interaction between the amide cores.[28,29] On the contrary, the band had a reversible change and recovered the absorption upon cooling.

Figure 9 depicts a schematic drawing of the molecular packing of P-C1 in the columnar nematic phase and P-Cm (m = 4, 8, 12) in the smectic A phases at ambient temperature. For P-C1 with the columnar nematic LC order, a relatively strong hydrogen bonding existed among the rigid amide cores within the rodlike polymer chain. As described by the mesogen-jacketed model, the whole polymer chain acted as a supramolecular rod to form the nematic phase. Meanwhile, for P-C4, P-C8, and P-C12 with the smectic LC ordering, hydrogen bonding also formed among the amide cores, and yet the polymer chain took a more sheetlike conformation to pack into the smectic structures.

To investigate the mechanism of the development of the liquid crystalline phases at molecular levels, 2D IR was performed to probe the sequential order of changes of chemical groups in the backbone and side chain with respect to temperature change. We chose P-C1 as an example because the vibrational bands of the alkyl end chains for other P-Cm polymers were overlapped with those of the backbone, while the $-OCHH_3$ stretching modes of P-C1 were independent from the alkyl C−H stretching modes of the backbone. On the other hand, although the liquid crystalline phase of P-C1 was different from those of the others, the interactions between the chemical groups were similar. Figure 10 presents two sets of FTIR spectra of P-C1 at different temperatures between 80 and 280 °C for heating and cooling processes. For the sake of clarity, spectra with a 20 °C interval are shown. According to Noda's rule,[22,30,31] the 2D IR correlation spectroscopy provides 2D synchronous and 2D asynchronous spectra. $\Psi(\nu_1/\nu_2)$ is defined as the cross-peak in an asynchronous spectrum, and $\Phi(\nu_1/\nu_2)$ is the cross-peak in a synchronous spectrum. When $\Phi(\nu_1/\nu_2) > 0$, if $\Psi(\nu_1/\nu_2)$ is positive, ν_1 varies prior to ν_2; if $\Psi(\nu_1/\nu_2)$ is negative, ν_1 varies after ν_2. And the sequence is reversed when $\Phi(\nu_1/\nu_2) < 0$. We concentrated on the region 3450−2811 cm^{-1} which presented the C−H vibration of P-C1. It should be noted that all the absorbance bands decreased

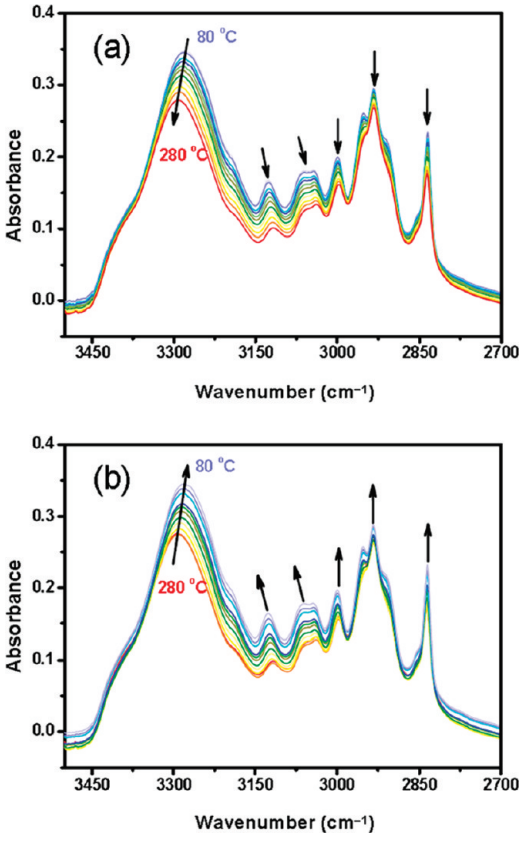

Figure 10. FTIR spectra of P-C1 in the 3500−2700 cm^{-1} region between 80 and 280 °C during heating (a) and cooling (b).

Table 3. Assignments of Infrared Frequencies for P-C1 at Ambient Temperature[25,26,28,32]

peak position (cm^{-1})	assignment
3281	ν(N−H) in amide bonds
3126, 3043	ν_{ar}(CH) in the aromatic ring
2999	$\nu_{as}(CH_3)$ of $-OCHH_3$
2933	$\nu_{as}(CH_2)$ of $-CH_2-$ in backbone
2835	$\nu_s(CH_3)$ of $-OCHH_3$

gradually with increasing temperature, and a reverse change was observed during the subsequent cooling process. According to the 1D WAXD results and the analysis mentioned before, the spectral data sets during heating and cooling were used separately for the 2D IR correlation analysis in the temperature range 80−280 °C.

The bands located at 3281, 3126, 3043, 2933, and 2835 cm^{-1} represented the characteristic vibrations of chemical groups in P-C1. The band assignments are listed in Table 3. The cross-peaks that appeared in synchronous and asynchronous maps were calculated by 2D IR, and the results are summarized in Tables 4 and 5. Signs of each cross-peak in the synchronous and asynchronous maps are shown in the top left corner of the tables, with the signs in the asynchronous map in parentheses. The reversed signs of their products are shown in the lower right corner.

According to the calculated 2D IR results in Table 4, during the heating process, the sequential order of spectral intensity changes was $\nu(CH_3)$ of $-OCHH_3 \rightarrow \nu$(CH) in the aromatic

Table 4. Change Sequence of Chemical Groups in ν(C−H) Region (3500−2700 cm^{-1}) during Heating[a]

ν_2 \ ν_1	3281	3126	3043	2933	2835
2835	+ (–)	+ (–)	+ (–)	+ (–)	
2933	+ (+)	+ (+)	+ (+)		+
3043	+ (–)	+ (+)		–	+
3126	+ (–)		–	–	+
3281		+	+	–	+
sequence	2835 → 3126 → 3043 → 3281 → 2933				

[a] Calculated from 2D maps within the temperature range 80−280 °C during heating.

Table 5. Change Sequence of Chemical Groups in ν(C−H) Region (3500−2700 cm^{-1}) during Cooling[a]

ν_2 \ ν_1	3281	3126	3043	2933	2835
2835	+ (+)	+ (+)	+ (+)	+ (–)	
2933	+ (+)	+ (+)	+ (+)		+
3043	+ (+)	+ (+)		–	–
3126	+ (+)		–	–	–
3281		–	–	–	–
sequence	3281 → 3126 → 3043 → 2835 → 2933				

[a] Calculated from 2D maps within the temperature range 80−280 °C during cooling.

ring → ν(N−H) in amide bonds → ν(C−H) of polymer backbone. In other words, in this temperature range 80−280 °C, the response of the chemical groups began from the end groups in the mesogenic units, followed by the movement of the benzene rings of the mesogenic cores. Because the end groups were individually connected to the mesogenic units at the peripheral position, they had larger freedom than the rigid amide cores and the backbones, and the side-chain hydrogen bonding gradually decreased in strength or even dissociated upon heating. The backbone had a delayed response compared with the side chains attaching to it because of the restriction by side-chain hydrogen bonding among the rigid amide cores in the side chains.

On the basis of the results listed in Table 5, during the cooling process, the motional order of the chemical groups was discerned as ν(N−H) in amide bonds → ν(CH) in the aromatic ring → ν(CH_3) of −$OCHH_3$ → ν(C−H) of polymer backbone. The ν(N−H) in amide bonds responded first, which drove the neighboring mesogens to interact with one another. The strengthening of the hydrogen bonding further stabilized the LC phase. The motions of the connected benzene rings and end groups followed the movement of the amide bonds. The backbone was still the last to respond to the temperature change.

The sequences obtained from the 2D IR analysis suggested the molecular mechanism in forming the LC phases. During the heating and cooling processes, the polymer backbone of P-C1 responded later than the chemical groups in the side chains because the backbone could not change its conformation easily owing to the attractive interactions among the side chains. This was different from the case of poly{2,5-bis[(4-methoxyphenyl)-oxycarbonyl]styrene} (PMPCS) which had the similar chemical structure but with the ester linkages in the side chains. For PMPCS, the backbone changed its conformation more easily to adopt the helical conformation after the phase transition to form the columnar phase because of the independent side chains.[32]

To confirm the role of hydrogen bonding in the formation and stabilization of the mesophases of P-Cm's ($m \geq 4$), we also analyzed the spectra data set of P-C12 in the region 3450−3000 cm^{-1} during the cooling process. The sequential order was also discerned as ν(N−H) in amide bonds → ν(CH) in the aromatic ring, which was the same as that in P-C1 without considering the vibration of CH_2 because of the overlapped absorptions of the alkyl tails and backbone. The earlier response of the amide bonds enabled the recovery of hydrogen bonding among the side chains, resulting in the enhanced rigidity of the side chains. On the other hand, the increased content of alkyl tails for these P-Cm ($m \geq 4$) polymers promoted the microphase separation between the alkyl tails and the rigid cores of the side chains, consequently stabilizing the smectic phases. In addition, the role of hydrogen bonding in the formation and stabilization of LC phases was also the reason for the similar transition temperatures of P-C4, P-C8, and P-C12 from variable-temperature WAXD experiments.

■ CONCLUSIONS

In summary, we found that hydrogen bonding could be applied to construct new MJLCPs and control their phase structures. MJLCPs with amide linkages in the side groups were synthesized via conventional radical polymerization. The polymer with methoxy end groups, P-C1, formed a columnar nematic

phase, while P-C4, P-C8, and P-C12 with longer alkyl tails formed smectic A phases. In addition to being affected by the length of the alkoxy peripheral chains, the phase structures of the polymers were also influenced by the side-chain hydrogen bonding. The new MJLCPs with side-chain hydrogen bonding may become potential functional materials as liquid crystalline elastomers and engineering plastics owing to their stable mesophase structures.

AUTHOR INFORMATION

Corresponding Author

*E-mail: fanxh@pku.edu.cn (X.-H.F.); zshen@pku.edu.cn (Z.S.); zhumf@dhu.edu.cn (M.-F.Z.).

ACKNOWLEDGMENT

Financial support from the National Natural Science Foundation of China (Grants 50925312, 50973016, and 20990232), the Programme of Introducing Talents of Discipline to University (No. 111-2-04), and National "973" Project (2011CB606004) is gratefully acknowledged.

REFERENCES

(1) Kato, T. *Science* **2002**, *295*, 2414–2418.
(2) Demus, P. D.; Goodby, P. J.; Gray, P. G. W.; Spiess, P. H.-W.; Vill, D. V.; Goodby, J. W.; Gray, G. W. In *Handbook of Liquid Crystals*; Wiley-VCH: Berlin, 2008; pp 17−23.
(3) Finkelmann, H.; Rehage, G. In *Liquid Crystal Polymers II/III*; Academic Press: New York, 1984; pp 99−172.
(4) Zhou, Q. F.; Li, H. M.; Feng, X. D. *Macromolecules* **1987**, *20*, 233–234.
(5) Chen, X.-F.; Shen, Z.; Wan, X.-H.; Fan, X.-H.; Chen, E.-Q.; Ma, Y.; Zhou, Q.-F. *Chem. Soc. Rev.* **2010**, *39*, 3072–3101.
(6) Tu, H.; Wan, X.; Liu, Y.; Chen, X.; Zhang, D.; Zhou, Q.-F.; Shen, Z.; Ge, J. J.; Jin, S.; Cheng, S. Z. D. *Macromolecules* **2000**, *33*, 6315–6320.
(7) Yin, X.-Y.; Ye, C.; Ma, X.; Chen, E.-Q.; Qi, X.-Y.; Duan, X.-F.; Wan, X.-H.; Cheng, S. Z. D.; Zhou, Q.-F. *J. Am. Chem. Soc.* **2003**, *125*, 6854–6855.
(8) Chen, X.; Tenneti, K. K.; Li, C. Y.; Bai, Y.; Zhou, R.; Wan, X.; Fan, X.; Zhou, Q.-F. *Macromolecules* **2005**, *39*, 517–527.
(9) Chen, S.; Gao, L.-C.; Zhao, X.-D.; Chen, X.-F.; Fan, X.-H.; Xie, P.-Y.; Zhou, Q.-F. *Macromolecules* **2007**, *40*, 5718–5725.
(10) Chai, C.-P.; Zhu, X.-Q.; Wang, P.; Ren, M.-Q.; Chen, X.-F.; Xu, Y.-D.; Fan, X.-H.; Ye, C.; Chen, E.-Q.; Zhou, Q.-F. *Macromolecules* **2007**, *40*, 9361–9370.
(11) Gopalan, P.; Andruzzi, L.; Li, X.; Ober, C. K. *Macromol. Chem. Phys.* **2002**, *203*, 1573–1583.
(12) Hammond, M. R.; Mezzenga, R. *Soft Matter* **2008**, *4*, 952–961.
(13) Whitesides, G. M.; Grzybowski, B. *Science* **2002**, *295*, 2418–2421.
(14) Pollino, J. M.; Weck, M. *Chem. Soc. Rev.* **2005**, *34*, 193–207.
(15) Binder, W. H.; Zirbs, R. In *Hydrogen Bonded Polymers*; Springer-Verlag: Berlin, 2007; Vol. 207, pp 1−78.
(16) Cornelissen, J. J. L. M.; Donners, J. J. J. M.; de Gelder, R.; Graswinckel, W. S.; Metselaar, G. A.; Rowan, A. E.; Sommerdijk, N. A. J. M.; Nolte, R. J. M. *Science* **2001**, *293*, 676–680.
(17) Bohle, A.; Brunklaus, G.; Hansen, M. R.; Schleuss, T. W.; Kilbinger, A. F. M.; Seltmann, J.; Spiess, H. W. *Macromolecules* **2010**, *43*, 4978–4985.
(18) Yu, H.; Shishido, A.; Li, J.; Kamata, K.; Iyoda, T.; Ikeda, T. *J. Mater. Chem.* **2007**, *17*, 3485–3488.
(19) Zhang, D.; Zhou, Q. F.; Ma, Y. G.; Wan, X. H.; Feng, X. D. *Polym. Adv. Technol.* **1997**, *8*, 227–233.
(20) Zhang, D.; Liu, Y.-X.; Wan, X.-H.; Zhou, Q.-F. *Macromolecules* **1999**, *32*, 5183–5185.
(21) Xu, Y.; Yang, Q.; Shen, Z.; Chen, X.; Fan, X.; Zhou, Q. *Macromolecules* **2009**, *42*, 2542–2550.
(22) Noda, I. *J. Am. Chem. Soc.* **1989**, *111*, 8116–8118.
(23) Chen, S.; Zhang, L.-Y.; Gao, L.-C.; Chen, X.-F.; Fan, X.-H.; Shen, Z.; Zhou, Q.-F. *J. Polym. Sci., Part A: Polym. Chem.* **2009**, *47*, 505–514.
(24) Zhao, Y.-F.; Fan, X.-H.; Wan, X.-H.; Chen, X.-F.; Yi; Wang, L.-S.; Dong, X.; Zhou, Q.-F. *Macromolecules* **2006**, *39*, 948–956.
(25) Skrovanek, D. J.; Howe, S. E.; Painter, P. C.; Coleman, M. M. *Macromolecules* **1985**, *18*, 1676–1683.
(26) Xue, C.; Jin, S.; Weng, X.; Ge, J. J.; Shen, Z.; Shen, H.; Graham, M. J.; Jeong, K.-U.; Huang, H.; Zhang, D.; Guo, M.; Harris, F. W.; Cheng, S. Z. D.; Li, C. Y.; Zhu, L. *Chem. Mater.* **2004**, *16*, 1014–1025.
(27) Pang, D.; Wang, H.; Li, M. *Tetrahedron* **2005**, *61*, 6108–6114.
(28) Kutsumizu, S.; Mori, H.; Fukatami, M.; Naito, S.; Sakajiri, K.; Saito, K. *Chem. Mater.* **2008**, *20*, 3675–3687.
(29) Shi, J.; Wu, P.; Yan, F. *Langmuir* **2010**, *26*, 11427–11434.
(30) Noda, I. *Appl. Spectrosc.* **1993**, *47*, 1329–1336.
(31) Noda, I.; Dowrey, A. E.; Marcoli, C.; Story, G. M.; Ozaki, Y. *Appl. Spectrosc.* **2000**, *54*, 236–248.
(32) Shen, Y.; Chen, E.; Ye, C.; Zhang, H.; Wu, P.; Noda, I.; Zhou, Q. *J. Phys. Chem. B* **2005**, *109*, 6089–6095.